Examination of Tuning Concepts Using Rubber Mounts

Undergraduate Honors Thesis

Presented in Partial Fulfillment of the Requirements for

Graduation with Honors Research Distinction in the

Department of Mechanical Engineering at

The Ohio State University

By:

Benjamin M. Joodi

Advisor: Dr. Rajendra Singh

Co-Advisor: Dr. Jason T. Dreyer

****

The Ohio State University

March 2013

Defense Committee:

Dr. Rajendra Singh

Dr. Jason T. Dreyer

Dr. Robert Siston

Abstract

Rubber mounts are common components within automotive vehicle powertrains and suspensions. They provide compliance at joints between substructures as well as provide vibration isolation between structures. These mounts are often designed to certain stiffness and damping values within a given frequency range. Narrow band tuning with regards to dynamic stiffness is difficult to achieve using mechanical force transmission elements without the incorporation of internal hydraulic elements. This project analytically and experimentally investigates the feasibility of rubber mount designs without hydraulic elements that have a notch-type behavior in its dynamic stiffness near 100-125 Hz over a frequency range of 0 to 500 Hz, with a dynamic stiffness range between 50 and 500 N/mm, and with a maximum mass of 5 kg. Based on these constraints, multiple dynamic stiffness component-level models (with displacement input and force output) are examined analytically. A prototype is designed, fabricated, and evaluated using finite element analysis and experimental testing. The prototype evaluation shows notch-type behavior in its transmitted force through the mount in a bench experiment; however, future evaluation is still required to evaluate the load capacity of the component and determine its effect within a system-level environment.

Acknowledgements

It is really important that I thank everyone that has helped me throughout the course of this project. I have had the privilege to work under both Dr. Rajendra Singh and Dr. Jason Dreyer. I would like to thank Dr. Rajendra Singh for giving me the opportunity to work on this project. Dr. Jason Dreyer has been more than grateful in offering assistance throughout this study. I would also like to thank Dr. Robert Siston for taking the time to review this thesis and being a member of my defense committee. Lastly, I would like to thank the College of Engineering for their support of this work.

Table of Contents

List of Figures

List of Tables

Chapter 1: Introduction

1.1 Background

Elastomeric mounts and bushings are used for isolation between two substructures or to accommodate misalignments among components. A typical rubber mounts consist of mainly metal (steel or aluminum), rubber and a support structure to connect it to substructures or components within vehicle systems.

Figure 1. 1: Common rubber mount bushing used in vehicle suspension. [1]

Mounts can be tuned based on different requirements of the application. For instance, if a mount has low stiffness and high damping then it will isolate the driver and passenger from feeling affects due to vibration. Likewise, if a mount has high stiffness and low damping then the car may handle more responsively. It is easily noticed that there is a tradeoff; therefore, the engineer will have to compromise the damping and stiffness based on the specific situation.

A specific local frequency range where dynamic stiffness needs to be attenuated in vehicle suspension components is an area of interest for manufactures. Hydraulic circuits and electrical circuits have known models that can attenuate specific frequencies where resonances

occur. Mechanical systems can potentially have the same effect if modeled correctly. This could be accomplished by varying the parameters of mechanical force transmission elements between two subsystems. If a resonance is observed in the subsystem response, a force transfer element separating the subsystem from other subsystems can attenuate the magnitude of the force transmitted at the resonant frequency. A notch filter has the capabilities of passing many frequency ranges except for a selected local range. In this situation, a notch filter is used to pass all frequencies except for the resonant frequency.

Viscous and hysteretic damping will be considered for this study. Viscous damping is used to describe a system where effective force is proportional to velocity, which is typical of systems where resistance is caused by viscous drag of a fluid. This is a common way to characterize damping force, but this is not entirely accurate for structural materials, and a rubber mount is considered a structural material. Even though viscous damping is not completely accurate for a rubber mount, it can still be used to approximate rubber mount behavior for a specific frequency range.

Hysteretic damping assumes that damping force is proportional to displacement, with a storage component in phase with the displacement and a dissipative component 90 degree out of phase or lagging with the displacement input. Figure 1.2 shows how the imaginary and real components of the dynamic stiffness are related. Where K_d is the dynamic stiffness magnitude, φ is the phase, K'' is the dissipative component of the dynamic stiffness, and K' is the storage component of the dynamic stiffness.

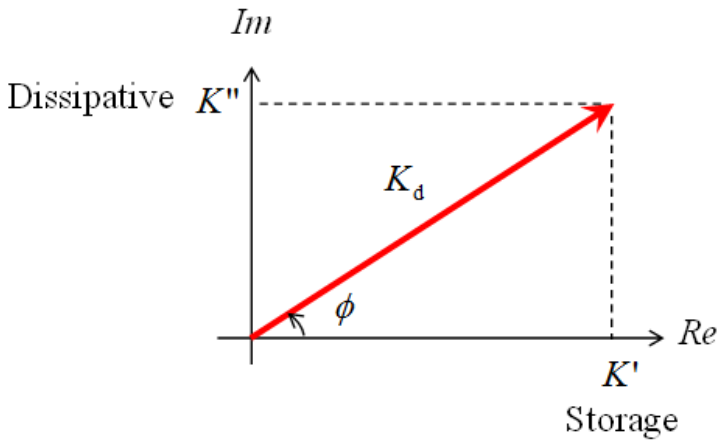

Figure 1. 2: Relationship between dissipative and storage elements for dynamic stiffness with hysteretic damping

Hysteretic or structural damping is defined as the damping caused by friction between internal planes slipping and sliding as a material is deformed [2]. Hysteretic damping incorporates the idea of hysteresis. Hysteresis is the phenomenon where its current state depends on its past state. The energy that is dissipated due to hysteresis is the area within the hysteresis loop of a stress versus strain plot. Rubber often displays this type of damping behavior rather than viscous damping for higher frequencies.

1.2 Literature Review

Literature has shown that mechanically tuned isolators can be used to attenuate specific resonant frequencies associated with the system in which it is integrated [3]. As already stated, electrical and hydraulic circuits can be easily used to create this notch filter behavior. An electrical circuit that can create this behavior could consist of an arrangement of a resistor, capacitor and inductor. Solving for the voltage output over the voltage input can obtain a response similar to the one shown in Figure 1.3. Equation 1 shows the transfer function that is formed by solving the system of Figure 1.3 in the frequency domain.

$$\frac{V_o}{V_i} = \frac{s^2 + 1/L_i C}{s^2 + \frac{R}{L_i}s + \frac{1}{L_i C}} \quad (1)$$

Where V_i is the voltage input measured across the resistance R, inductance L_i, and capacitance C. The output voltage $V_{o,}$ is measured over the inductor and capacitor. The impedance in the Laplace domain with complex frequency s, is found for each circuit element. The voltage V_o and V_i in Figure 1.3, and the relative impedance due to each circuit element is then used to create the transfer function, Equation 1. By tuning the systems inductance, capacitance, and resistance with the correct values, a notch filter can be graphed between magnitude and frequency. An example of values that could be used to create an electrical circuit notch filter is listed in Table 1.1.

Table 1. 1: RLC circuit values for notch filter response in Figure 1.3

Parameters	Units	Values
L	H	.05
C	F	9.00E-04
R	Ω	1

Incorporating notch filter characteristics with rubber mounts can be very useful with attenuating specific frequencies that may excite resonance while driving.

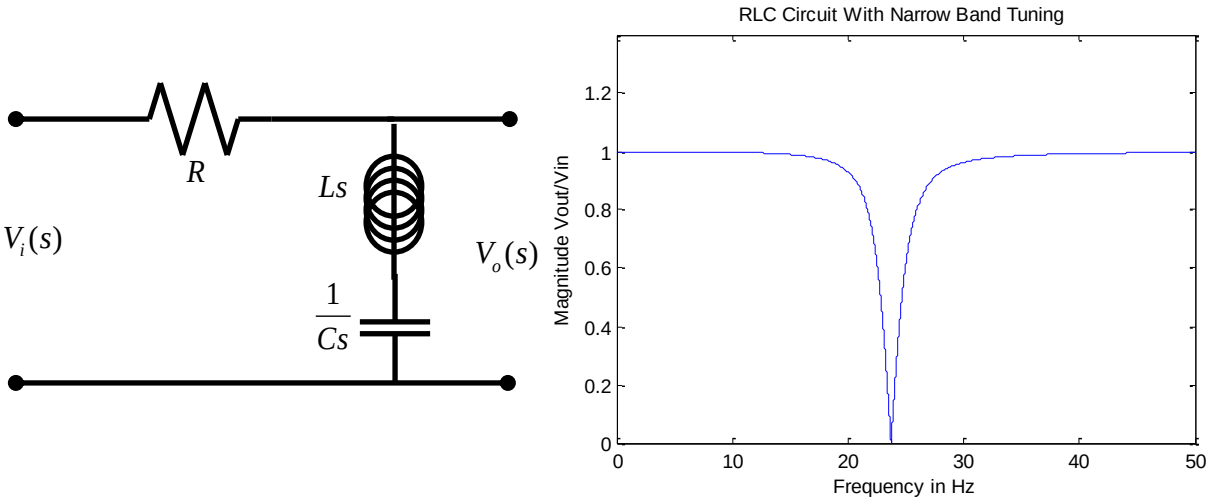

Figure 1. 3: Electrical circuit that can be used to form magnitude response with notch filter characteristics.

Hydraulic circuits can also be tuned to attenuate a certain frequency range. Mounts that incorporate the use of hydraulic circuits tuned to these frequencies can produce narrow band tuning to increase energy dissipation [3,4]. These hydraulic mounts incorporate an inertia track that allows fluid to pass from an upper chamber to a lower chamber of the mount for high amplitude excitation. This inertia is chosen so that it observes resonance at the natural frequency of the engine mount. There is damping that is associated with this track which allows the hydraulic mount to act as a tuned damper [5]. Another benefit of hydraulic mounts includes the decoupler typically associated with the design. This decoupler acts as a low resistance path between the upper and lower chambers for small dynamic stiffness amplitude excitation. This short circuits the flow of the fluid through the decoupler rather than flowing through the inertia track at small amplitudes. The benefits that come from this allows for the mount to be both good for control and handling [5]. This is a desirable characteristic that manufactures look for in mount design. The basic design of a hydraulic mount is shown on Figure 1.4.

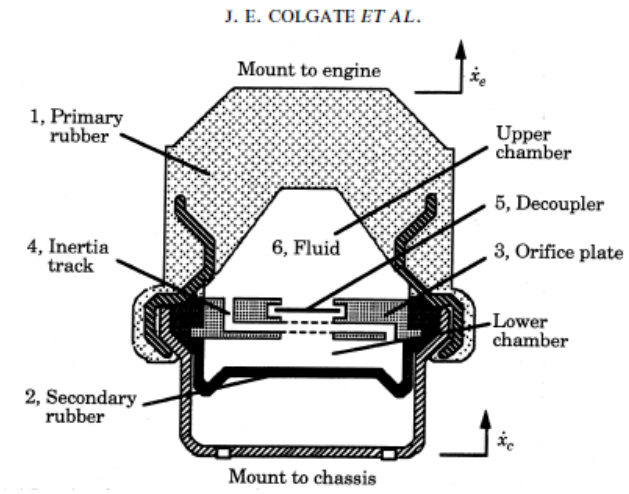

Figure 1. 4: Basic design of a hydraulic mount [5]

Problems that are associated with the use of hydraulic mounts are that they are typically more expensive than rubber mounts, and there is a certain complexity to the design and manufacturing process that makes this approach less desirable by manufactures. Incorporating this notch filter behavior in strictly mechanical elements would be a desirable alternative.

Tuned mass absorbers can be created using strictly mechanical elements as well. A single degree of freedom system composed of a mass element with a spring and damper can help show this concept, shown in Figure 1.5.

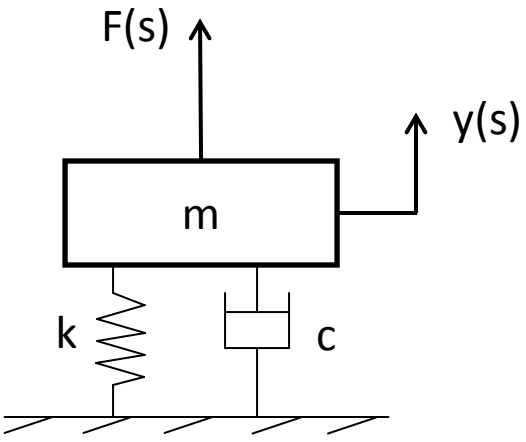

Figure 1. 5: Single degree of freedom model

The driving point method, which is used to describe the behavior of a system where the response is measured at the same point as the measured input excitation, is used to solve for Equation 2.

$$\frac{y(s)}{F(s)} = \frac{1}{ms^2 + cs + k} \tag{2}$$

Where *y(s)/F(s)* is the output over input response solved in the Laplace domain, which is in compliance units. *F* is the input excitation force, *y* is the output displacement, *m* is the mass, *k* is the stiffness of the spring, and *c* is the damping associated with the mass. Equation 2 is the transfer function *y(s)/F(s)* for Figure 1.5. By solving for the magnitude and using the values in Table 1.2, the solid line in Figure 1.7 can be plotted.

Table 1. 2: Values for single degree of freedom model

Parameters	Units	values
m	kg	1
c	Ns/m	1
k	N/m	100

Resonance would occur if an input excitation force was applied to the single degree of freedom system at 10 Hz. This is because the system would be disturbed at its natural frequency. In the case that this resonance is undesirable at this frequency, then an additional mass can be applied. The system would now have two degrees of freedom creating two natural frequencies. This system is shown in Figure 1.6

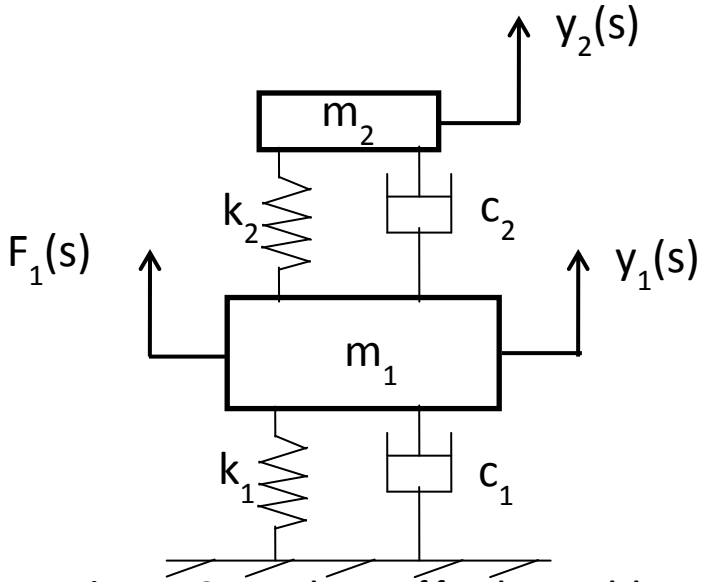

Figure 1. 6: Two degree of freedom model

By solving for the response $y_1(s)/F_1(s)$ in the Laplace domain, Equation 3 can be derived.

$$\frac{y_1(s)}{F_1(s)} = \frac{m_2 s^2 + c_2 s + k_2}{m_1 s^2 + (c_1 + c_2)s + k_1 + k_2)(m_2 s^2 + c_2 s + k_2)^2} \tag{3}$$

Where $y_1(s)/F_1(s)$ is the output over input of the response to Figure 1.6, y_1 is the displacement of the primary mass m_1, F_1 is the input excitation force, m_2 is additional mass, k_2 is the coupling spring, and c_2 is the coupling damper. By analyzing this model the same way as Figure 1.5, the magnitude response can be plotted in Figure 1.7. If an input excitation force is applied to the two degree of freedom system at 10Hz, resonance would no longer occur because the natural frequencies would not be disturbed. This is an example of mechanically tuned mass absorber. The values used for this mechanically tuned mass absorber with two degrees of freedom are tabulated on Table 1.3.

Table 1. 3: Values for two degrees of freedom model

Parameters	Values	Units
m_1	1	Kg
m_2	0.1	kg
c_1	1	Ns/m
c_2	0.1	Ns/m
k_1	100	N/m
k_2	10	N/m

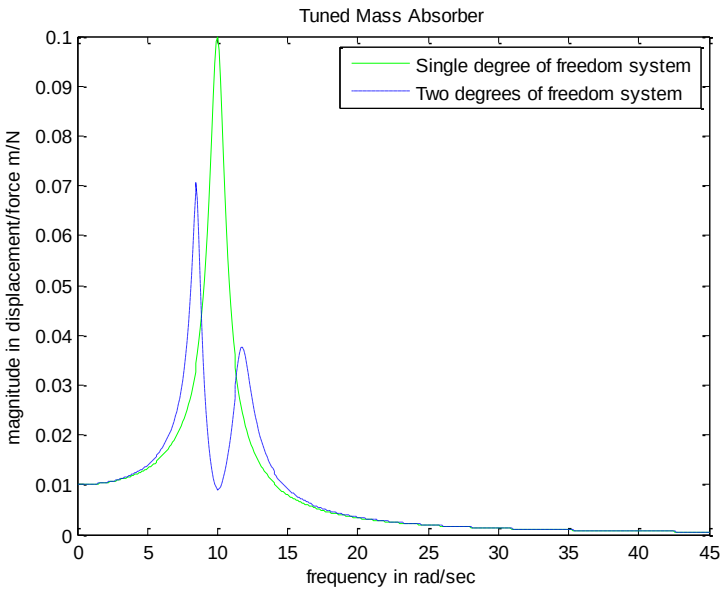

Figure 1. 7: Magnitude Response for single and double degree of freedom systems

There are various examples of mechanically tuned mass absorbers today. These are typically created by augmenting a mechanical system with additional mass and rubber tuned for specific frequencies. Some examples of where this has been accomplished are dish washer motors, half shafts on cars, engine flywheels and building heating and ventilation systems. These tuned mass dampers have similar characteristics to that of the hydraulic mount circuits.

This concept is difficult to integrate into a joint or structural vibration path. In this case, the problem requires a cross-point formulation.

The cross-point method is used to describe the behavior of a system where the response is measured at a different point than the measured input excitation. The cross-point method is mainly for interfacial elements, and the driving point method is for system level analysis. Figure 1.8 shows how using cross-point analysis and applying a displacement as an input to a simple single interfacial mass can produce the known behavior of a band-pass filter by using the correct values for the spring stiffness, damping, and mass. Equation 4 is the dynamic stiffness transfer function associated with the single interfacial mass system in Figure 1.8.

$$\frac{F}{x} = \frac{\left(k_1 + c_1 s\right)\left(k_2 + c_2 s\right)}{ms^2 + \left(c_1 + c_2\right)s + \left(k_1 + k_2\right)} \tag{4}$$

Where *F/x* is the dynamic stiffness, k_1 and k_2 are the spring stiffness, c_1 and c_2 are the damping and *m* is the mass associated with the model. Similar to that of the electrical circuit, mechanical systems in force transmissibility models have impedance as well. The damping and stiffness elements create "impedance" that resist the force being transmitted through the model.

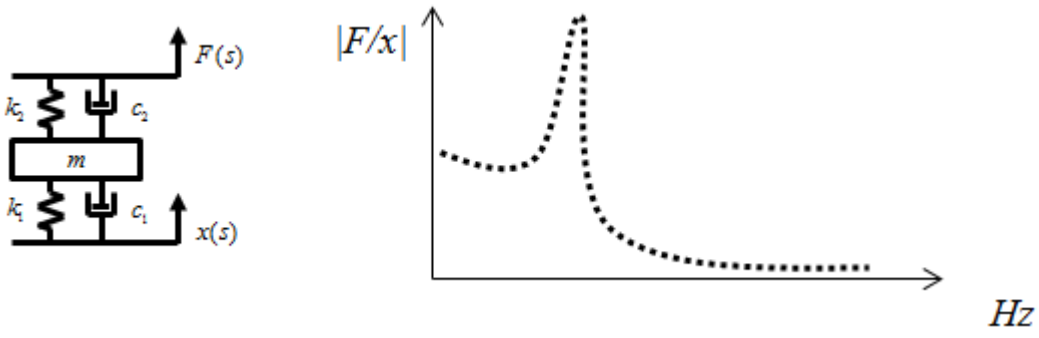

Figure 1. 8: Cross point method of single mass

By solving for the dynamic stiffness transfer function of the model and using the correct values for the stiffness, damping, and mass, a graph of the dynamic stiffness magnitude versus frequency can be created. This is shown in Figure 1.8. By understanding the dynamics of this system, superimposing this model with other inertial elements of similar form can possibly create narrowband tuning behavior. Chapter 2 will go more in depth of how narrowband tuning can be achieved using mechanical elements in a rubber mount.

Understanding the behavior of specific elastomeric material properties is a hurdle that makes creating the desired notch filter response in a rubber mount difficult. Elastomers exhibit both frequency and amplitude dependence (for both mean and dynamic loading) [3]. This means that it is important to experimentally validate any theoretical design with experimental models. Finite Element Analysis (FEA) is also a tool that can be used to give a quick approximation for the behavior a physical model. FEA is an approach for attaining an approximate solution to a complex problem by using numerical methods to break up the problem into more manageable elements [7].

1.3 Project Objective and Design Specification

The main intention of this research is to design a rubber mount with narrow band tuning characteristics in order to understand the physics and its practicability for the automotive industry. The automotive industry is interested in a variety of frequency ranges that affect both noise and vibration. However, for this study, we will focus on frequency ranges associated with resonances due to frame modes coupling with those modes of the vehicle suspension, say between 50 and 300 Hz. More specifically, we will try to target a narrow band frequency range near 100-125 Hz for this specific proof of concept. Tuning at lower frequencies, say below 50 Hz, is not achievable with mechanical mounts alone. Hydraulic mounts achieve high damping

values at the low frequencies by design, and as a result, the stiffness magnitude is actually higher at lower frequencies for these mounts. This effect cannot be well understood unless considering the entire system model. Hydraulic mounts/ elements are used for low frequency since they can achieve high inertia/ low stiffness values required to isolate/ tune lower frequencies. Mechanical systems would be too compliant or require too much mass at low frequency. It is a desirable characteristic that this rubber mount will only have a combined mass of less than 5 kg, which is a typical size for large hydraulic mounts. We will target a minimum attenuation of 3 dB in the notch frequency regime (which is considered a noticeable attenuation in terms of noise and vibration). Rubber dynamic stiffness values will be kept at around 50-500 N/mm. If hysteretic damping is considered, the hysteretic damping ratio (loss factor) will be kept under 0.4. These are the typical values on the low end of mount stiffness. After knowing the constraints related to the rubber mount, this study then shows the process to design, create, and test a rubber mount that has potential characteristics of a notch filter

The scope of the project is to investigate and provide a proof of concept for the design of a rubber mount with notch filter behavior. This study is organized to discuss specific steps in the design process and verification of the theoretical analysis by using experimental testing and FEA.

The specific objectives include:

1) Derive the analytical dynamic stiffness and associated modal model that has desired notch filter characteristics under the design constraints.
2) Propose a physical specimen with the dynamics suggested by the analytical models.
3) Evaluate the analytical modal model using FEA of the proposed physical specimen.

4) Construct the physical specimen and evaluate the dynamic force transmitted through the physical specimen. Compare the associated dynamic force through the specimen with the analytical dynamic stiffness model.
5) Propose of an automotive design concept based on the results of this study and additional issues that must be addressed for realization of such a concept.

Chapter 2: The Theoretical Design - Dynamic Stiffness

2.1 Dynamic Stiffness Problem Formulation

The cross-point method forms the basic approach for creating the theoretical dynamic stiffness model. By looking at Figure 1.8, the behavior of a single block system is known to produce a band-pass filter dynamic stiffness magnitude response. The method that is used to create a notch filter incorporates testing various arrangements of this simple single degree of freedom system and graphing the magnitude of the dynamic stiffness as a function of frequency. A demonstration of this idea is shown with Figure 2.1. Looking at the two different systems displayed, one can notice that two masses are in series in Figure 2.1 A and four masses are in parallel in Figure 2.1 B. It is assumed that superimposing the single block with multiple single blocks could potentially form the notch filter frequency responses as shown in both Figure 2.1 A and B. The rest of this chapter shows the analyses of various systems by changing values for the parameters and graphing the magnitude of the dynamic stiffness against the frequency in order to create the notch filter frequency response.

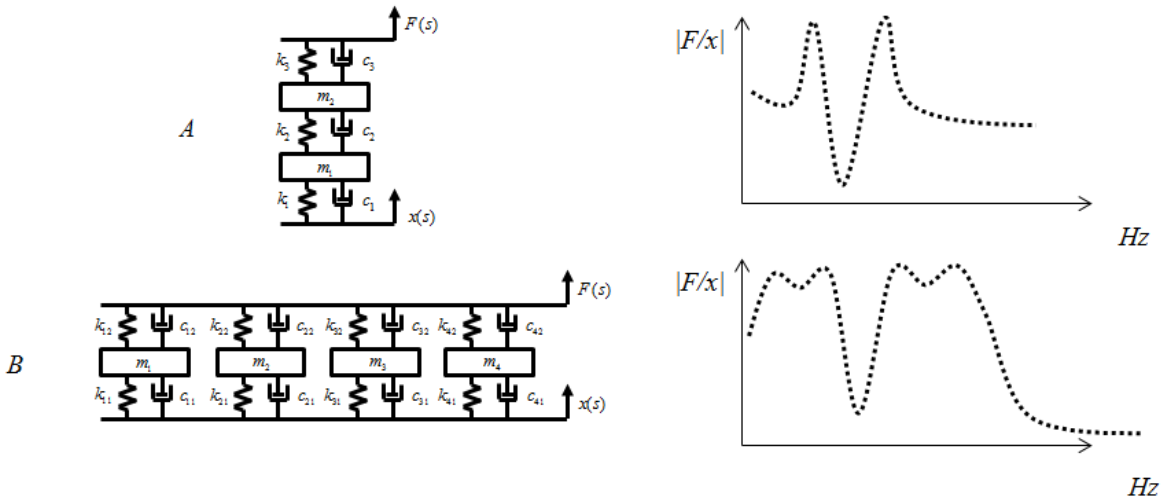

Figure 2. 1: A and B showing possible arrangements of spring mass spring systems that can potentially create a notch filter magnitude response

2.3 Viscous Versus Hysteretic Damping

Viscous damping was used to analyze models that were believed to potentially create this notch filter behavior, but in every case it proved to be unsuccessful. Viscous damping proves to be a good approximate for elastomeric materials for a small frequency range, but over a large frequency range it is difficult to obtain a desirable response that could be used for a notch filter. The models analyzed using viscous damping consisted of the single interfacial mass, two interfacial masses in series, multiple interfacial masses in parallel, and many more, but due to the characteristics of the equations of motion for viscous damping it was difficult to achieve a desired characteristic dynamic stiffness. Mathematically it can be shown how hysteretic damping and viscous damping are different.

The single degree of freedom system with harmonic excitation, Figure 2.2, shows the difference between viscous and hysteretic damping.

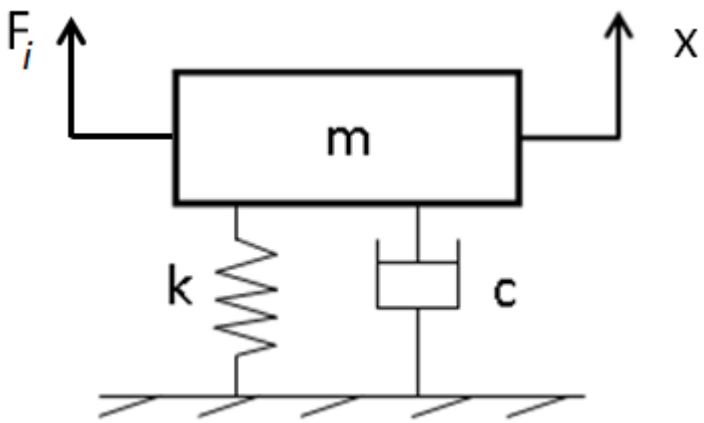

Figure 2. 2: Single block with one spring and one damper

$$mx(t) + c\dot{x}(t) + kx(t) = f_i(t) \tag{5}$$

$$x(t) = Xe^{j\omega t} \text{ and } f(t) = F_i e^{j\omega t} \tag{6}$$

$$(-m\omega^2 + jc\omega + k)X \cancel{e^{j\omega t}} = F_i \cancel{e^{j\omega t}} \tag{7}$$

$$c = \frac{jk\eta}{\omega} \tag{8}$$

$$\left(-m\omega^2 + k + \eta kj\right)X = F_i \tag{9}$$

Where m is the mass, k is the spring stiffness, c is the damping, j is $\sqrt{-1}$, ω is angular frequency, η is the hysteretic damping ratio, t is time, F_i is the amplitude of the input excitation force, $f_i(t)$ is the input excitation force, X is the displacement amplitude, and $x(t)$ is the displacement output. Equation 5 is the equation of motion in the time domain for viscous damping of the simple spring mass damper model in Figure 2.2. Equation 5 shows how the damping force is linearly related to the velocity. Utilizing the Laplace transform and converting Equation 5 into the frequency domain, Equation 7 can be derived. This is the equation of motion in the frequency domain for viscous damping. By using Equation 8 to substitute $\frac{jk\eta}{\omega}$ for c, the

equation of motion using hysteretic damping, Equation 9 is formed. Notice that hysteretic damping can only be analyzed in the frequency domain. By analyzing Equation 9, essential differences between hysteretic and viscous damping are discovered. Equation 9 shows that the damping is now proportional to the displacement but still in phase with the velocity. By using hysteretic damping equations of motion there was success in creating notch filter behavior for mechanical force transmissibility elements.

2.3 Hysteretic Damping Models

It has been noticed that structural materials behave more similar to models that have damping proportional to the displacement. Since elastomeric material is considered a structural material, the physical behavior should have strong correlation with the hysteretic equations of motion for a larger frequency range.

For the hysteretic damping models analyzed, it was known that increasing mass and decreasing stiffness would typically decrease the poles. The poles determined the location of the peaks on the dynamic stiffness magnitude versus frequency plots. Increasing the hysteretic damping ratio decreased the amplitude of the peaks. These characteristics were true for all models analyzed using hysteretic damping.

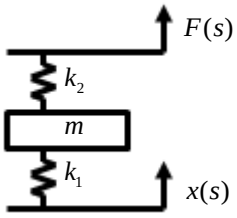

Figure 2. 3: Single Interfacial Mass

The theoretical equations of motions for all hysteretic damping models were placed into Matlab. The dynamic stiffness equation of motion for the single block transfer function is Equation 10.

$$\frac{F}{x} = \frac{k_1(1+\eta j)k_2(1+\eta j)}{m\omega^2 + k_1(1+\eta j) + k_2(1+\eta j)} \tag{10}$$

Where k_1 and k_2, are the stiffness of the springs, η is the hysteretic damping ratio associated with each spring, j is $\sqrt{-1}$, and ω is frequency. Equation 10 was used to verify that it was possible to produce band-pass filter behavior predicted from Figure 1.8. The values used to create the dynamic stiffness magnitude versus frequency response in Figure 2.4 are shown on Table 2.1 at the end of chapter 2.

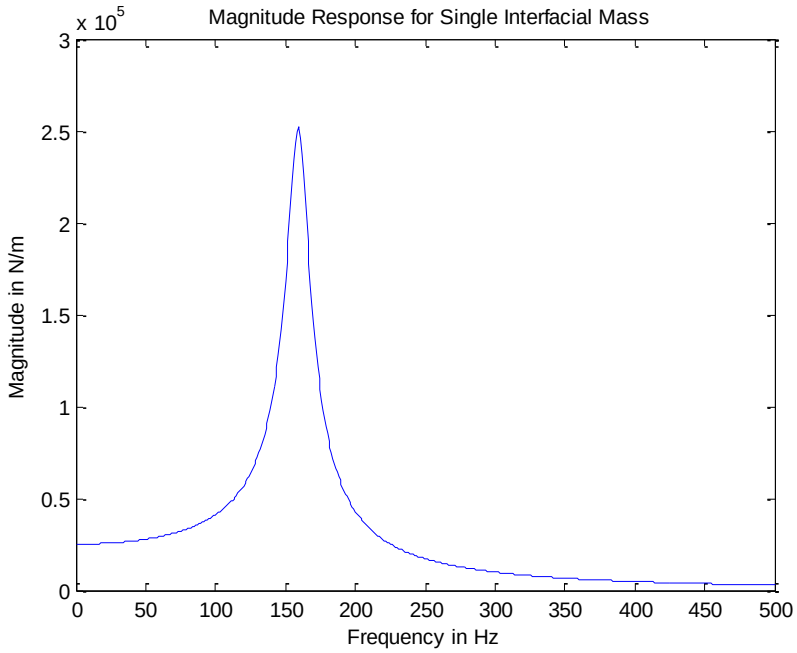

Figure 2. 4: Theoretical dynamic stiffness magnitude response for single mass

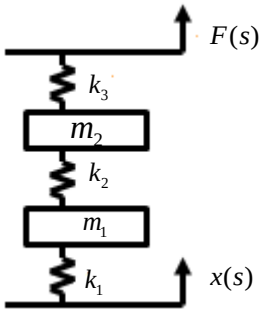

Figure 2. 5: Two interfacial masses in series

The next model analyzed using hysteretic damping was the two interfacial masses in series. The equation of motion used for this model is Equation 11.

$$\frac{F}{x} = \frac{k_1(1+\eta j)k_2(1+\eta j)k_3(1+\eta j)}{(m_1\omega^2 + k_1(1+\eta j) + k_2(1+\eta j)\left(m_2\omega^2 + k_2(1+\eta j) + k_3(1+\eta j)\right) - (k_2(1+\eta j))^2} \tag{11}$$

where k_1, k_2, and k_3 are the stiffness associated with each spring, η is the hysteretic damping ratio, j is $\sqrt{-1}$, and ω is frequency. The values used to create the plot in Figure 2.6 are tabulated in Table 2.1. There was no success creating a notch filter using the two interfacial masses in series. The peak occurring at higher frequencies typically was a large percentage lower than the peak occurring at lower frequencies while using a constant hysteretic damping ratio. It was also very difficult in attenuating the frequency in between the two peaks more than that of the frequencies outside of the two peaks.

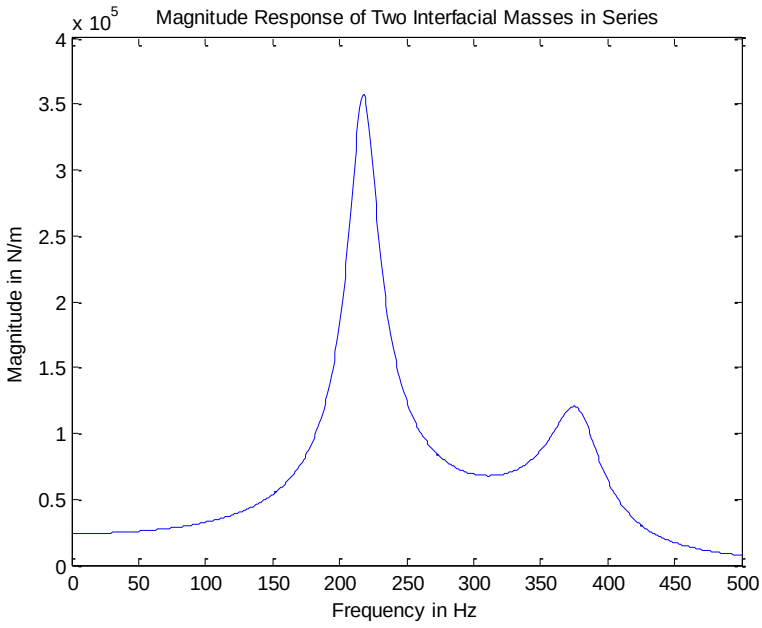

Figure 2. 6: Theoretical dynamic stiffness magnitude response for two interfacial masses in series

There was more success creating a notch filter while analyzing the multiple masses in parallel. While modeling this system, it became apparent that creating a notch filter would be possible. After placing one bandpass filter on a magnitude versus frequency plot, adjusting the placement of another right next to it was easily done by either slightly changing the mass value or stiffness coefficients. The equations of motion for the multiple interfacial masses in parallel was the same equation of motion for the single interfacial mass, only there are mulitple added together. For Figure 2.7, thirteen masses in parallel were used to create the notch filter. This shows a notch at around 120 Hz which is in the targeted range of 100 to 125 Hz. The values used to create the response in Figure 2.7 are tabulated on Table 2.1. Graphing this plot led the motivation to begin testing whether a physical model and a FEA model would behave the same way.

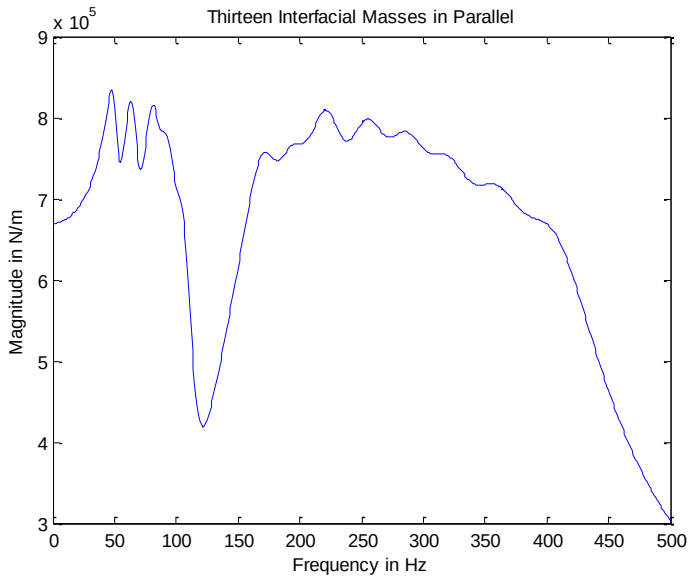

Figure 2. 7: Theoretical dynamic stiffness magnitude response for thirteen masses in parallel

In order to have a physically tractable model, the thirteen masses in parallel model was adjusted in order to simplify the testing phase for the FEA analysis and MTS 831.50 [8] elastomer test machine. In order to do this, five masses were used instead of thirteen. Since it was cut down to five masses, there would now be a smaller frequency range that was amplified. This is fine though, because amplifying later frequencies is easy to accomplish and not a significant amount of mass is required. The reduction of masses still illustrates the design, but simplifies the design. Figure 2.8 shows the new magnitude versus frequency plot using five masses in parallel. The new notch is now at around 110 Hz. Parameters used to create this model consisted of the values on Table 2.1.

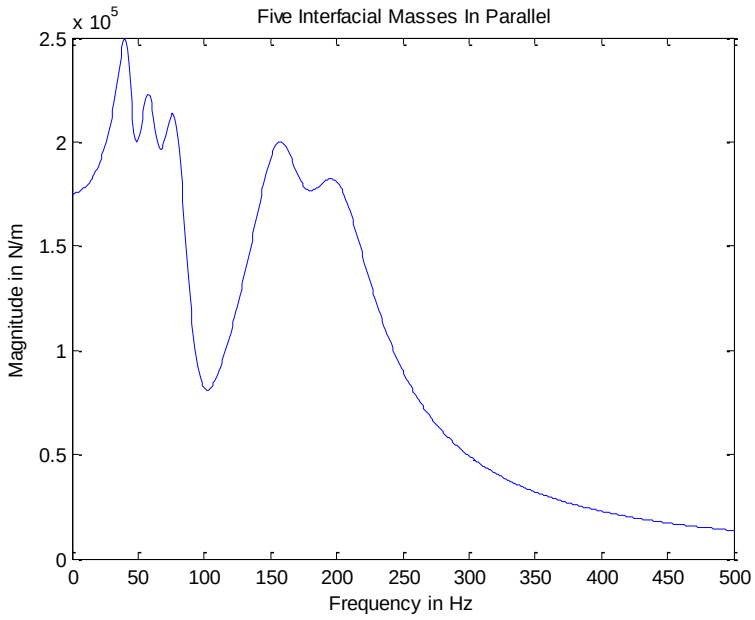

Figure 2. 8: Theoretical dynamic stiffness magnitude response for five masses in parallel

After successfully finding values that could be used to create the notch filter at around 100-125 Hz, it was necessary to find out how large of an effect changes in stiffness would affect the theoretical dynamic stiffness model. This was important because the elastic modulus of rubber is load and frequency dependent. In order to do this, the stiffness and damping parameters were increased, decreased, or arbitrarily changed by a factor of 10%. Plots of the resulting magnitude responses are shown on Figure 2.9 and Figure 2.10. Since there still seems to be a notch and five distinct peaks in both cases, the stiffness of the rubber used should not have significant changes if slightly inaccurate. After noticing this behavior, it was now time to test this model to verify that it would create a notch filter in an application setting.

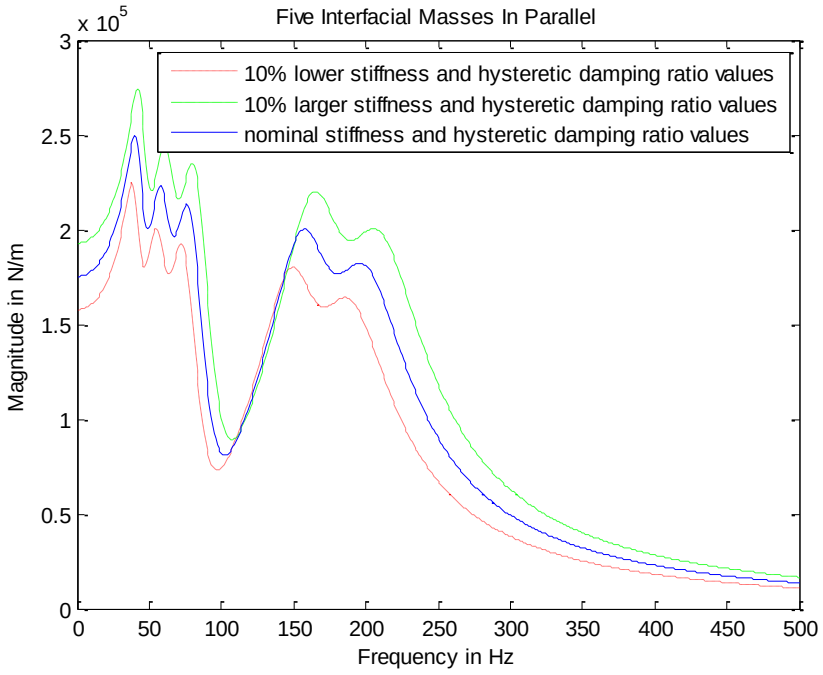

Figure 2. 9: Comparison of magnitude response of five interfacial masses in parallel having 10% larger, 10% lower and nominal stiffness and damping parameters

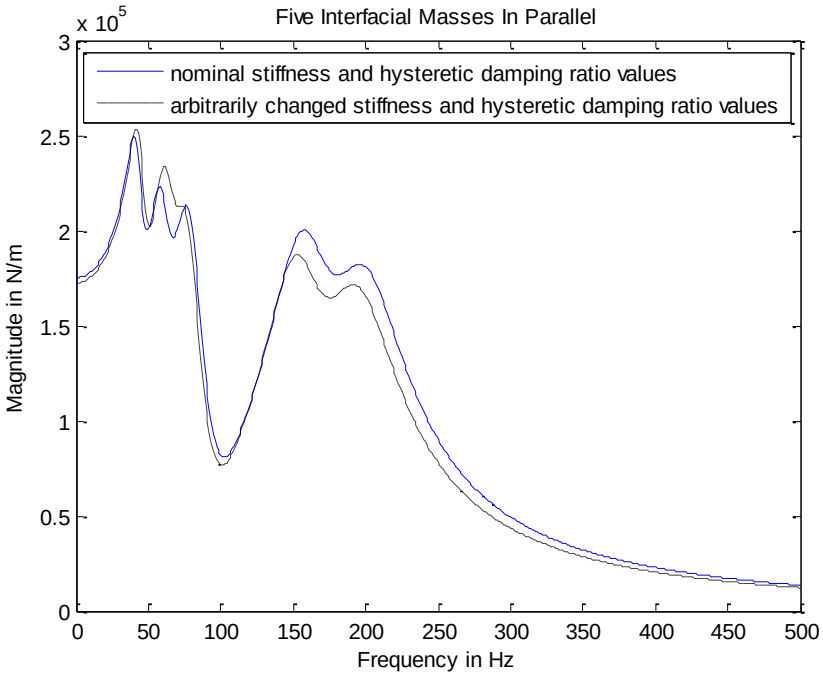

Figure 2. 10: Comparison of magnitude response of five interfacial masses in parallel having arbitrarily changed nominal stiffness and damping parameters by a factor of 10%

Table 2. 1: Values for hysteretic damping models

	Units	Model Values			
Parameters		Single Interfacial Mass	two Interfacial Masses in Series	13 Multiple Interfacial Masses in Parallel	5 multiple Interfacial Masses in Parallel
m_1	kg	0.1	1	.65	1.4
m_2	kg		0.05	.5	0.72
m_3	kg			.1275	0.155
m_4	kg			.0975	0.1
m_5	kg			.125	0.72
m_6	kg			0.875	
m_7	kg			0.0975	
m_8	kg			0.0775	
m_9	kg			0.0625	
m_{10}	kg			0.55	
m_{11}	kg			0.05	
m_{12}	kg			1.25	
m_{13}	kg			0.04	
k_1	N/mm	50	500		
k_2	N/mm	50	50		
k_3	N/mm		50		
k_{11}	N/mm			125	50
k_{12}	N/mm			50	50
k_{21}	N/mm			100	100
k_{22}	N/mm			75	75
k_{31}	N/mm			75	75
k_{32}	N/mm			75	75
k_{41}	N/mm			75	75
k_{42}	N/mm			72.5	75
k_{51}	N/mm			122.5	50
k_{52}	N/mm			122.5	50
k_{61}	N/mm			75	
k_{62}	N/mm			75	
k_{71}	N/mm			125	
k_{72}	N/mm			125	
k_{81}	N/mm			125	
k_{82}	N/mm			125	
k_{91}	N/mm			125	
k_{92}	N/mm			125	
k_{101}	N/mm			125	
k_{102}	N/mm			125	
k_{111}	N/mm			125	
k_{112}	N/mm			125	
k_{121}	N/mm			75	
k_{122}	N/mm			50	
k_{131}	N/mm			125	
k_{132}	N/mm			125	
η		0.1	0.1	0.2	0.3

Chapter 3: Physical Design Concept

3.1 FEA Model for Modal Analysis

After deriving an analytical dynamic stiffness model that had characteristics of a notch filter, validating the design was the next step. In order to create the FEA model, it was necessary to figure out the dimensions based on the important parameters calculated in the Matlab theoretical model. The FEA model was based on the stiffness used for the rubber, the mass sizes used for the steel, and the elastic modulus of the rubber that would be used for the physical test.

The rubber used for the physical and FEA model was ethylene propylene diene monomer (EPDM). Since EPDM rubber can have a varying elastic modulus of anywhere from 1-10MPa, it was necessary to find an exact value of the elastic modulus of the rubber used before testing. In order to obtain a value for the elastic modulus of the rubber, impulse hammer testing was used. Rubber sheets were cut into lengths of 12 mm with cross sections of 645 mm^2. A solid cylindrical steel block of weight 1.006 kg, diameter of 76.2 mm and thickness of 25.4 mm was applied on top of the rubber sheets. Two accelerometers were placed on top of the steel block and the steel block was struck with the impulse hammer. This test was completed using one rubber sheet under the steel block, and again using two rubber sheets under the steel block. The setup is shown on Figure 3.1.

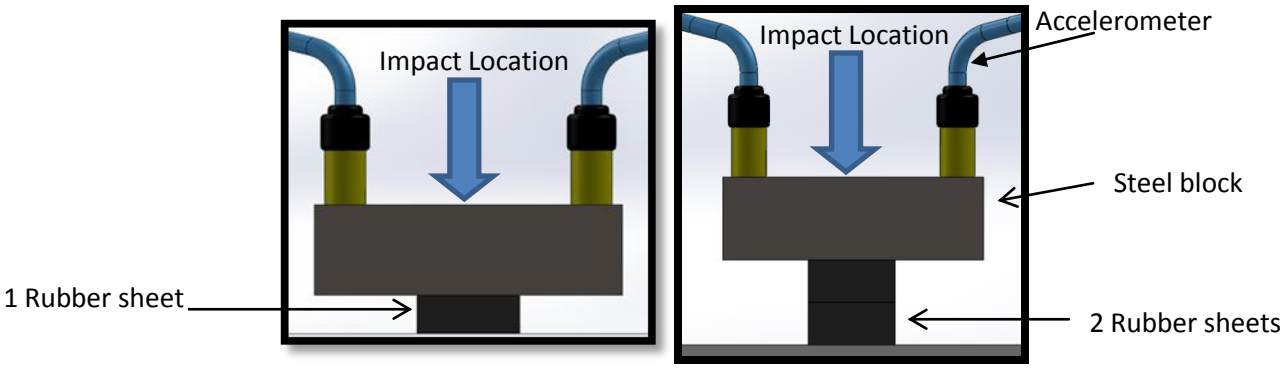

Figure 3. 1: Rubber testing set up for single rubber sheet and two rubber sheets stacked.

Two accelerometers were used in the test and each was strategically placed so that it was known where the vertical natural frequency occurred. The natural frequency in the vertical direction would be the natural frequency where both accelerometers were in phase.

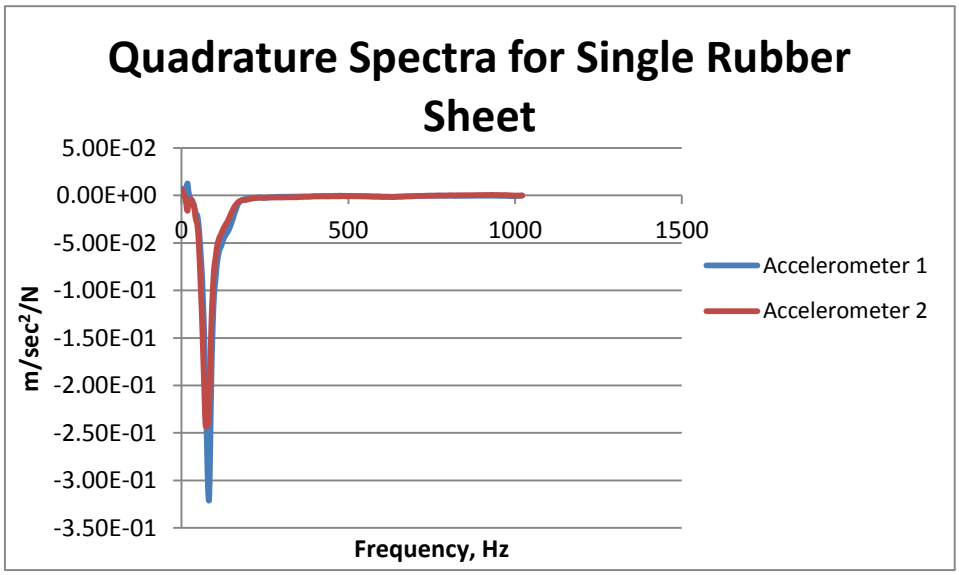

Figure 3. 2: Imaginary part of frequency response for single rubber sheet

By looking at the imaginary part of the frequency response in Figure 3.2 it is easy to notice that the natural frequency that occurs at about 80-100 Hz is the natural frequency in the

vertical direction because the two accelerometers are in phase. Since the natural frequency is now known and the mass of the steel block is known, the stiffness can be found using Equation 12.

$$k = m\omega_n^{\,2} \tag{12}$$

where ω_n is the natural frequency of the block supported by the rubber element, k is the stiffness of the rubber and m is the mass of the steel block. The magnitude response was then used to find the damping ratio of the rubber. By looking at Figure 3.3 and using the half power point method (Equation 14), the damping ratio was found to vary from being 0.1-0.2. The damping ratio calculation is shown using Equation 13

$$\frac{\Delta\omega}{2\omega_n} = \zeta \tag{13}$$

$$\Delta\omega = bandwidth\ of\ (\frac{\max amplitude}{\sqrt{2}}) \tag{14}$$

where ζ is the damping ratio.

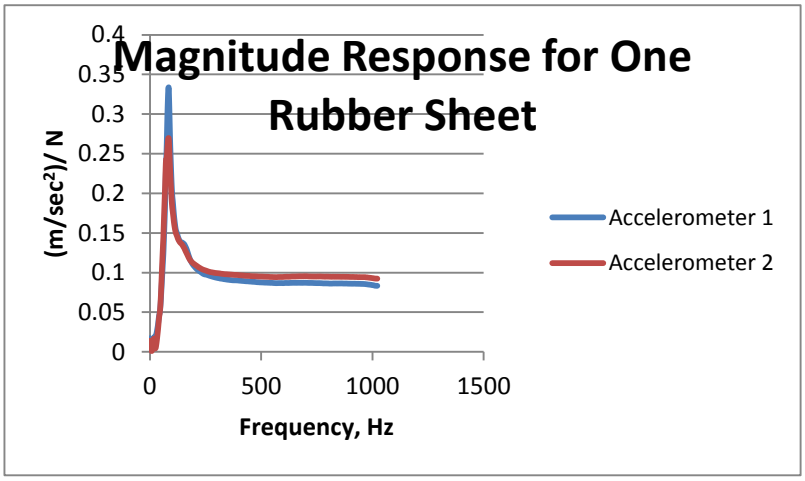

Figure 3. 3: Magnitude Response for One Rubber Sheet

This test was completed using a single rubber sheet and two rubber sheets glued. The magnitude response for the two rubber sheets glued is shown in Figure 3.4. The imaginary part of the frequency response was found to be similar to the single rubber sheet test. The largest amplitude peak on the magnitude response plot is the natural frequency where both accelerometers are in phase.

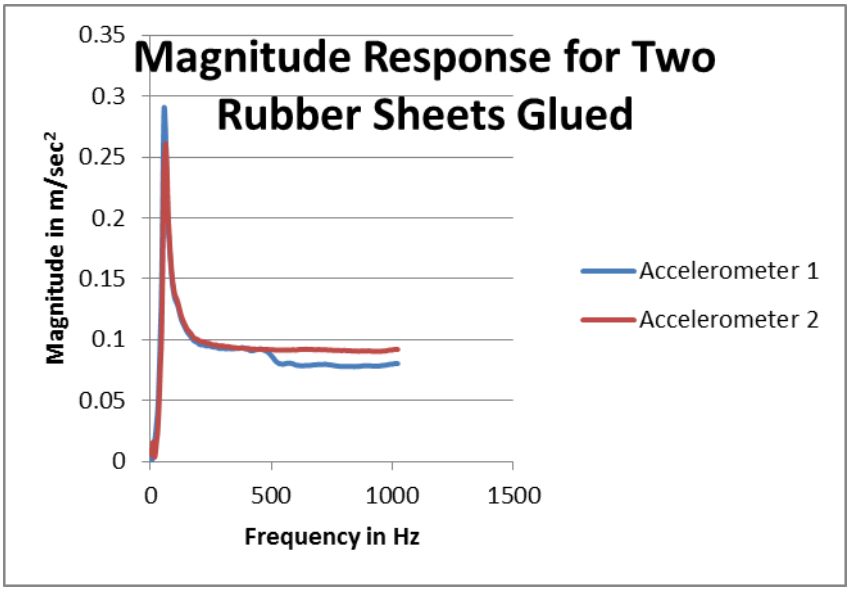

Figure 3. 4: Magnitude Response for Two Rubber Sheets Glued

By using the same approach as the single rubber sheet, the natural frequency, stiffness and damping ratios were found. The results for three trials for a single sheet, and two sheets glued are tabulated on Table 3.1.

Table 3. 1: Rubber testing results

	Test	Natural Frequency (Hz)	Viscous Damping Ratio	Stiffness (N/mm)
Single Sheet	Trial 1	85	0.118	287
	Trial 2	80	0.188	254
	Trial 3	70	0.157	195
	Average	**78**	**0.154**	**245**
Two Sheets Glued	Trial 1	66	0.197	173
	Trial 2	54	0.130	116
	Trial 3	56	0.196	125
	Average	**58**	**0.174**	**138**

Since the stiffness of a single rubber sheet was around double that of the stiffness for two sheets glued then it could be concluded that the glue did not have a significant affect on the stiffness of the rubber during the physical testing. This is because the only difference between the two tests was the effective rubber length. Looking at Equation 15, it is known that since the length of the rubber in the two rubber sheets glued test was twice the length of the rubber in the single rubber sheet test, then the stiffness would be twice as small. There may be a some error in the test simply because the cross sectional area was not exactly the same for the two rubber sheets glued. Equation 15 can be used to show how this would cause differences in stiffness values as well. The damping ratio for the rubber in all of the trials was around 0.1 to 0.2. A value of 0.3 was used for the hysteretic damping ratio in the theoretical case. The hysteretic damping ratio can be estimated as twice the viscous damping ratio for small amplitudes and relatively small values of damping. It should be noted that it is difficult to predict damping ratio values by using a magnitude response plot.

Using the data from the impulse hammer test, it is possible to find the elastic modulus for the rubber used by using Equation 15.

$$k = \frac{EA}{L_r} \tag{15}$$

where E is the elastic modulus, A is the loaded area, and L_r is the thickness. By knowing the area of the cross sections for the rubber to be .645 mm^2, the length of the rubber sheet to be 12mm, and the measured stiffness of the rubber sheet to be oround 250 N/mm, the elastic modulus was found to be 4.65 MPa. The Young's modulus of the rubbers was 4.65 MPa and the stiffness values were defined in the Matlab code. After knowing these two values, square

cross sections with reasonable lengths were used to create the rubber masses needed to have duplicate properties of the theoretical model. The values are placed on Table 3.2.

Table 3. 2: Rubber spring parameters

Spring #	Stiffness (N/mm)	Area (mm^2)	Length (mm)
11	50	11.8X11.8	13
12	50	11.8X11.8	13
21	100	16.7X16.7	13
22	75	14.5X14.5	13
31	75	14.5X14.5	13
32	75	14.5X14.5	13
41	75	14.5X14.5	13
42	75	14.5X14.5	13
51	50	11.8X11.8	13
52	50	11.8X11.8	13

The same procedure was taken for the steel masses for the model. The density of the steel was 7800 kg/m^3 and the steel mass sizes were used from the Matlab code. The steel masses have rectangular cross sections. These values are listed on Table 3.3. After knowing this information the appropriate lengths and areas needed were calculated to create the FEA model. The computer aided design model is shown on Figure 3.5.

Table 3. 3: Steel mass parameters

Steel Mass #	Mass (kg)	Density (kg/ m^3)	Volume (cm^3)	Area (mm^2)	Length (mm)
1	1.400	7800	180	50.8X69.9	50.8
2	0.720	7800	90	25.4X71.1	50.8
3	0.155	7800	20	15.2 X25.4	50.8
4	0.100	7800	13	10.2X25.4	50.8
5	0.720	7800	90	25.4X71.1	50.8

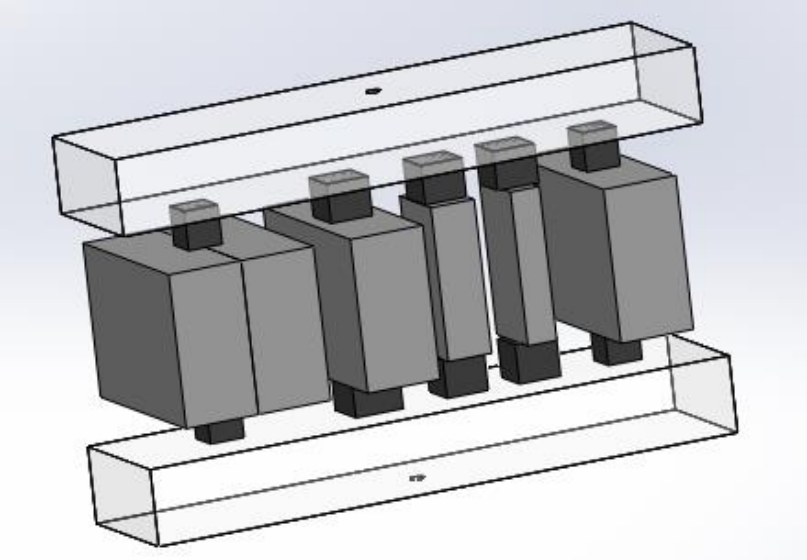

Figure 3. 5: Computer aided design model that would be used for FEA

3.2 The FEA Analysis – Verification of Modal Properties

Acrylic support plates were added to the top and bottom to provide a constrained surface for the FEA analysis and experimental testing using the MTS Elastomer Test Machine. Acrylic was chosen because it is light weight and very stiff. The acrylic was created to be 203.2 mm X 25.4 mm X 50.8 mm. Also, a frequency analysis was applied to the acrylic to make sure that no bending would occur below 950 Hz. If bending occurred, there would be additional degrees of freedom that would affect the system. After doing this analysis, a linear dynamic modal analysis of the entire model was completed in order to obtain the undamped frequencies associated with the poles of the system.

The modal analysis consisted of creating constraints that would simulate the dynamics of the theoretical stiffness model. This meant creating roller supports to all of the faces perpendicular to the horizontal direction, so that no motion could occur in the horizontal

direction. Also, in order to solve for the poles, the top and bottom surfaces of the acrylic were fixed. The model used for the harmonic analysis is shown on Figure 3.6.

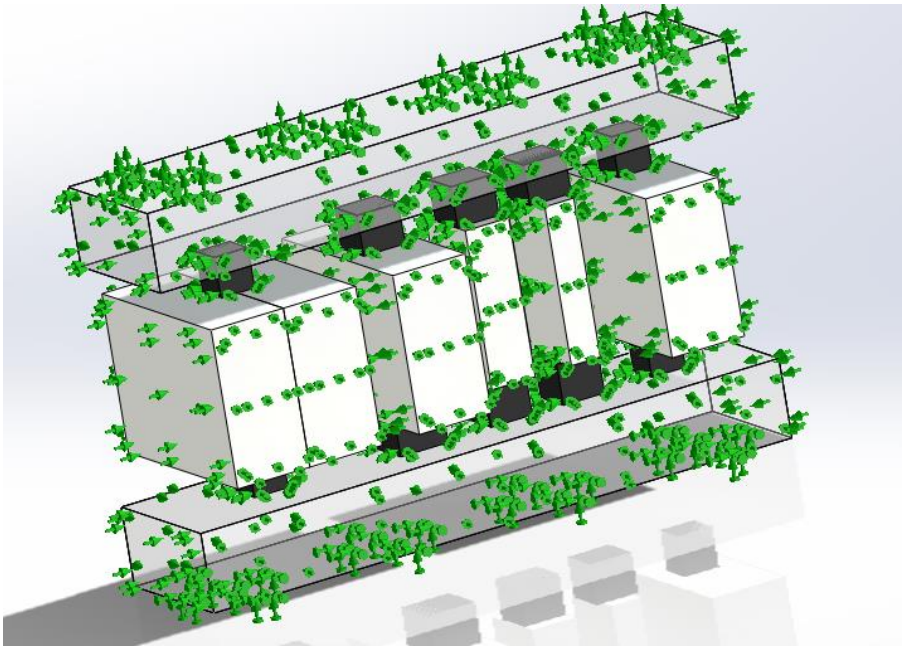

Figure 3. 6: Model used for linear dynamic harmonic modal analysis

The results of the FEA modal analysis are listed in Table 3.4, and they are compared with the poles of the theoretical modal model.

Table 3. 4: Differences between theoretical and FEA poles

Pole Frequency #	Frequency (Hz) From FEA Modal Model	Frequency (Hz) From Theoretical Modal Model	$F_{theo} - F_{FEA}$
1	43	42	1
2	62	60	2
3	82	81	1
4	160	163	3
5	195	209	14

From looking at the $|F_{theo}-F_{FEA}|$ of Table 3.4, it is easy to notice that there are a lot of similarities between the FEA and the theoretical modal models. Good observations from this data are that all of the poles are relatively similar. Pole number 5 has the most error between the theoretical and FEA. Mass number four was found to create this pole. The rubber cross sectional area associated with this mass was not completely covered. Since the cross sectional area was not completely covered, the stiffness would decrease. It was also found that the pole would decrease with decreasing stiffness. This corresponds well with the differences between the two frequencies on Table 3.4. Figure 3.7 shows how the cross sectional area of the rubber was not completely covered by the mass. It is important to note that the FEA model and analytical model in this section are not a dynamic stiffness models. They are modal models of the setup used to verify the assumption that the rubber blocks will behave like springs, required for later formulation of a dynamic stiffness model

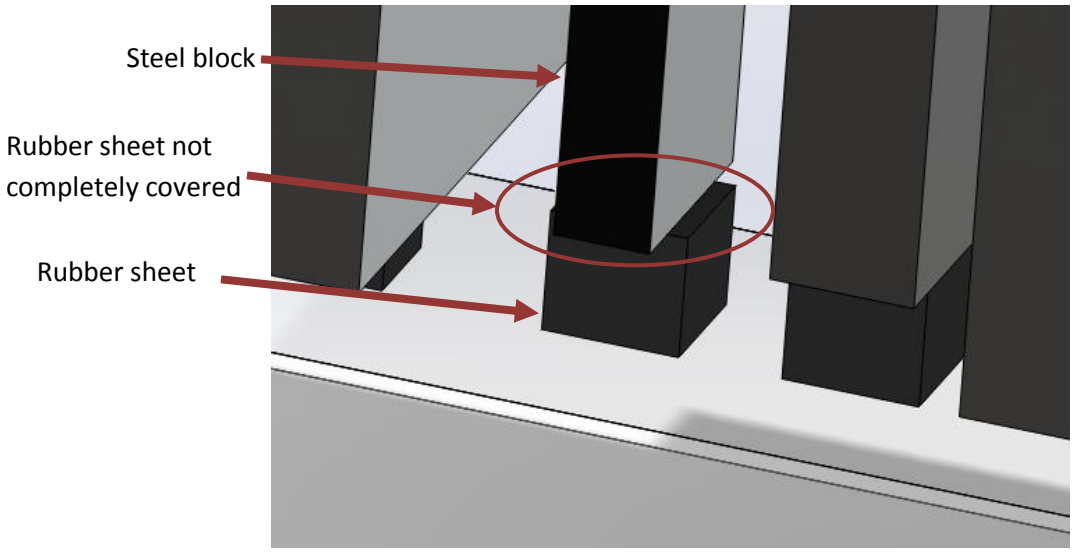

Figure 3. 7 Shows why pole number 5 of FEA differed from theoretical

Chapter 4: Experimental Testing of Physical Model – Dynamic Stiffness

In order to test an experimental model, a physical model had to be created. This model replicates the same dimensions as that of the FEA model. Figure 4.1 shows the physical model that would be used for experimental testing.

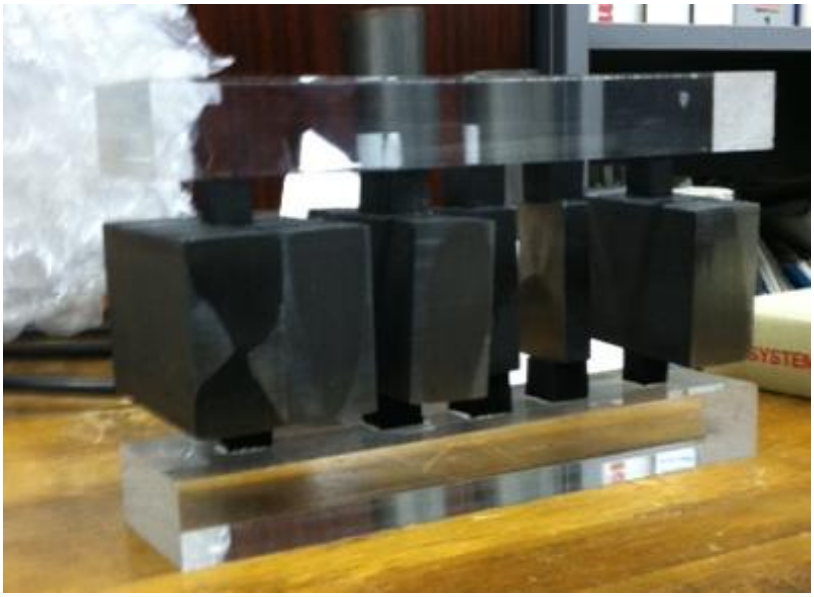

Figure 4. 1: Physical Model

The technique in testing the physical model would be by using a MTS 831.50 Elastomer Test System. The constrained theoretical analysis completed in chapter two for multiple masses in parallel would be accurate for how this would be tested. The MTS 831.50 Elastomer Test System would input a frequency to the model. Depending on the frequency, the model would vibrate more if it caused resonance in the system. A plot is made of the force output versus frequency of the model (Figure 4.2).

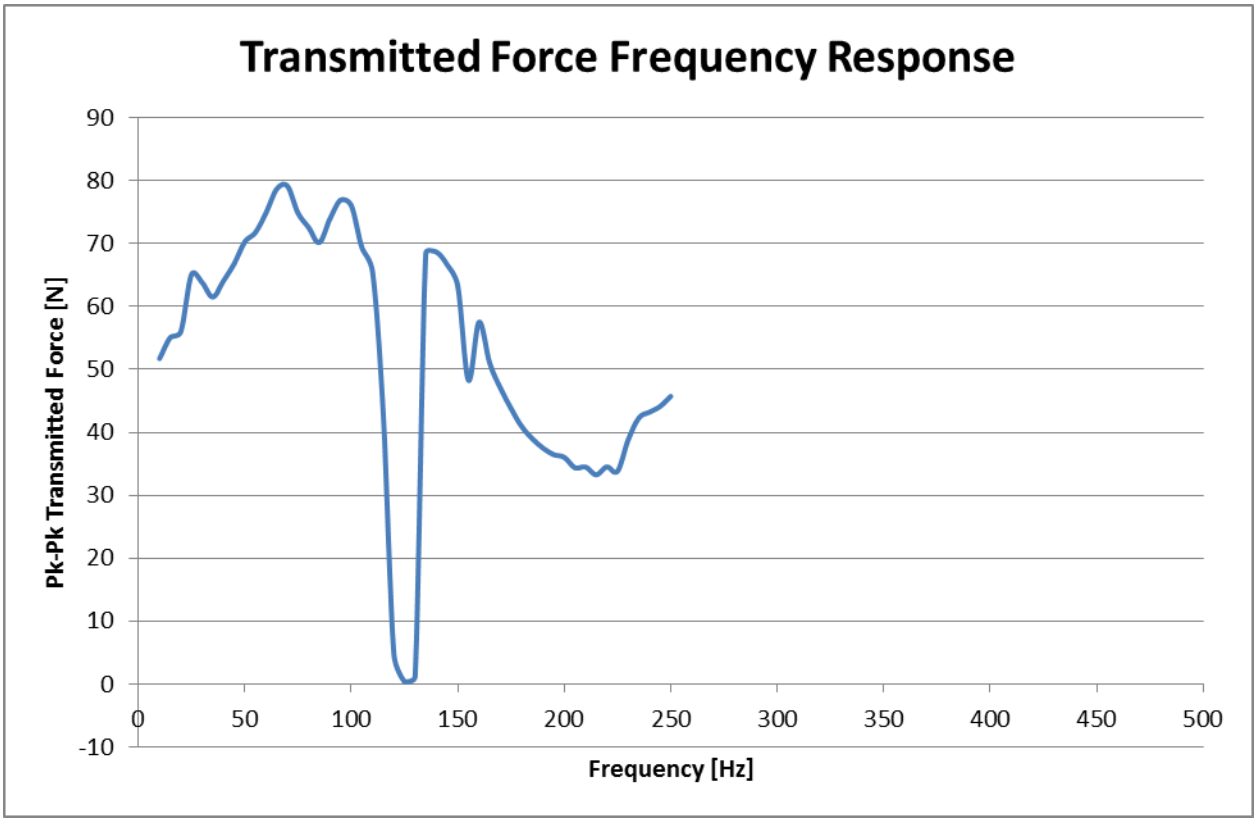

Figure 4. 2: The force transmitted versus frequency response using the MTS 831.50 Elastomer Test System

The results shown in Figure 4.2 have similarities to the theoretical dynamic stiffness results. There is a notch at around 125 Hz, which is nearly out of the range of 100-125Hz, but the design could be easily modified to change this behavior. Additional mass could be added to the system to fix this by redistributing the pole and zeros of the dynamic stiffness model. Another great observation for Figure 4.6 is the occurrence of all five peaks. It is easy to distinguish that there are five peaks with each occurring at 30 Hz, 70 Hz, 97 Hz, 140 Hz and 164 Hz. The difference between the theoretical and experimental dynamic stiffness characteristic peak frequencies is shown in Table 4.1.

Table 4. 1: Comparison between theoretical and experimental results – characteristic peak frequencies of dynamic stiffness

Pole Frequency #	Frequency (Hz) From Experimental Measurements	Frequency (Hz) From Dynamic Stiffness Analytical Model	$\left\|F_{theo} - F_{\exp}\right\|$
1	30	42	12
2	70	60	10
3	97	81	16
4	140	163	23
5	164	209	45

These results could help determine whether creating rubber mounts for the automotive industry to attenuate specific frequency ranges could be applicable. This model fits the constraint requirements of being less than 5 kg, dynamic stiffness values of 50-500 N/mm and having a hysteretic damping ratio under 0.4. An optimization approach, not included in the scope of this work could be used to modify the design for better characteristics. This could help reduce the weight even more to make the design more practical and economical in terms of excess weight and material cost.

The experimental follows the same trend as the theoretical dynamic stiffness results. The most error occurs for peak frequency number four and five. The main reason for this error most likely comes from the design set up for the physical model. The cross sectional area of the rubber sheets connected to mass three and four were not completely covered by the steel masses. This would change the values for the stiffness since stiffness is dependent on cross sectional area. Since there was less cross sectional area, the experimental stiffness would actually be less than the theoretical. Lower stiffness also implies that there would be a lower peak frequency associated with these two interfacial masses. Table 4.1 data seems to agree with this possible

source of error. If this experiment was run again, the entire rubber cross sectional area would need to be covered by the steel mass to get the most accurate results. Another source of error while testing the specimen seemed to be that the machine may have had issues controlling amplitudes near 125 Hz. This is partially to blame for such low amplitude force. It shows the trend where it should be, but the test must be rerun in displacement amplitude control around that point to get accurate characterization. This is noticeable because of how large the attenuation is on Figure 4.2 at around 125 Hz. The theoretical model only calculated an attenuation of about 3 dB whereas Figure 4.2 shows a force attenuation to 0 N. A last source of error is the material properties used in the model, as they may have been estimated at different displacement amplitudes as seen in testing.

Chapter 5: Design Concept for Vehicle Application

After the FEA and experimental testing, it was decided to develop a conceptual design that could be used as a prototype for vehicle applications. This prototype would have all of the same properties as the physical model used for testing purposes. Like the testing model, this prototype would have five steel masses in parallel and a total of ten rubber masses, one on each side of the steel masses. This prototype would also have two support base plates, but instead of making these out of acrylic each would be made out of steel. Figure 5.1 shows a collapsed view of the prototype. The steel masses are cylindrical in shape and the smaller masses fit within the bigger ones. All of the rubber masses are O-rings in shape except for the two smallest ones which are solid cylinders. These rubbers fit on the top and bottom edges of the steel masses. In order to get a better understanding of how this prototype was designed an exploded view is also shown for convenience. This is shown in Figure 5.2.

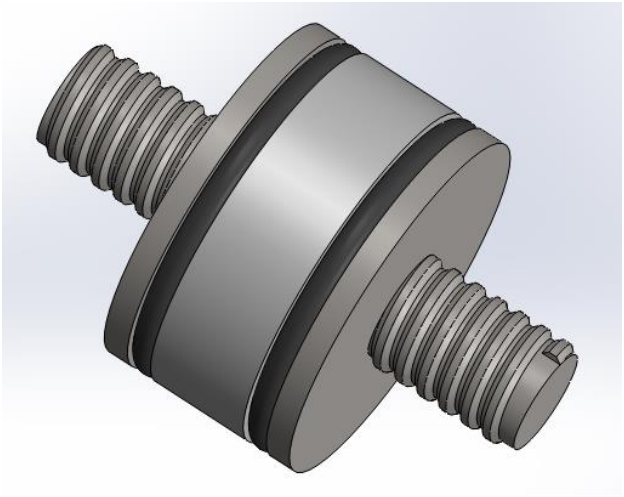

Figure 5. 1: Collapsed view of design concept

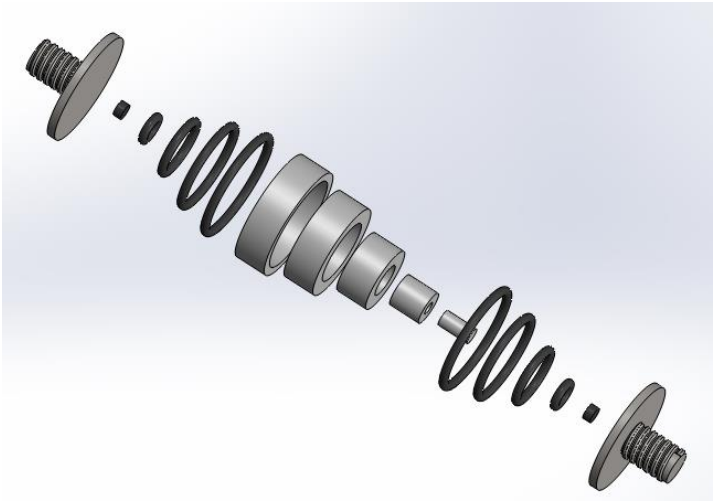

Figure 5. 2: Exploded view of design concept (darker components denote rubber, lighter components denote metal)

Chapter 6: Conclusions

An important goal of this research was to simply gain a better understanding of the physics that are associated with the rubber mount with tuned dynamic stiffness. This was accomplished by designing, fabricating and testing a model for a rubber mount that could potentially have narrowband tuning behavior. This study shows evidence that it is possible to

create rubber mounts with notch filter characteristics using reasonable parameters. The theoretical, FEA and experimental results for the constrained model all show similar behavior for notch filter characteristics. Future research efforts can come up with solutions to optimize the design of these rubber mounts so that continuous improvements of existing designs for mounts can be used in the automotive industry.

This research will have important contributions for future research efforts which could potentially make the driving experience more tolerable for drivers and less expensive for manufacturing industries. This will make for a safer and less harsh driving experience since rubber mounts can potentially attenuate frequencies of resonance due to structural interactions. Rubber mounts would then be a commercially viable alternative to hydraulic mounts for this notch filter characteristic. If further research and an optimization study are completed for a rubber mount design, it will be known whether this would be a good decision for the automotive industry to focus their time on for better isolator mount concepts. Other issues that still need to be addressed include temperature dependence, humidity, age, amplitude dependence, size constraints, off-axis coupling, and testing with other materials rather than just EPDM. All of these issues will need to be addressed, in the context of a specific application, before rubber mounts with narrow band tuning characteristics can be used in commercially viable vehicle suspension.

The information gained from this study will be shared with automotive industry to further research possible solutions. These results can also be used to validate different software codes, which are used in design of elastomeric components, as well as gain valuable insight into physics of tuned elastomeric mounts of this type.

References

[1] "Super Soft Rubber Mountings - To 20 Lbs." Super Soft Rubber Mountings - To 20 Lbs. N.p., n.d. Web. 28 Feb. 2013

[2] Shivaprasad.P. "Hysteretic Damping." Scribd. N.p., n.d. Web. 1 Mar. 2013. <http://www.scribd.com/doc/30395428/Hysteretic-Damping>.

[3] Park, J. Y. and R. Singh, "Vibration Analysis of Powertrain Mounting System with a Combination of Active and Passive Isolators with Spectrally-Varying Properties," SAE Int. Journal of Passenger Cars - Mechanical Systems, 2(1), 1312-1322, 2009.

[4] Barszcz, B., J.T. Dreyer, and R. Singh, "Experimental Study of Hydraulic Engine Mounts using Multiple Inertia Tracks and Orifices: Narrow and Broad Band Tuning Concepts," Journal of Sound and Vibration 331, 5209-5223, 2012.

[5] Colgate, J. E., C. T. Chang, Y. C. Chiou, W. K. Liu, and L. M. Keer. "Modelling of a Hydraulic Engine Mount Focusing on Response to Sinusoidal and Composite Excitations." Journal of Sound and Vibration 184.3 (1995): 503-28. Print

[6] Gil-Negrete, N., J. Vinolas, and L. Kari, "A Simplified Methodology to Predict the Dynamic Stiffness of Carbon-black Filled Rubber Isolators Using a Finite Element Code," Journal of Sound and Vibration, 296, 757-76, 2006.

[7] "FINITE ELEMENT ANALYSIS." Finite Element Analysis. N.p., n.d. Web. 3 Mar. 2013. <http://www.stress.com/servicetier3.php?pid=75>.

[8] "Elastomer Test Systems." *MTS*. N.p., n.d. Web. 15 Mar. 2013. <http://www.mts.com/en/products/producttype/test-systems/load-frames uniaxial/servohydraulic/elastomer/index.htm>.

Appendix A: List of Symbols

k	spring Stiffness coefficient [N/m]
c	viscous damping coefficient [Ns/m]
m	mass of block [kg]
x	output displacement for force transmissibility elements [m]
L_i	inductance coefficient [L]
ω	angular frequency [rad/sec]
C	capacitance coefficient [F]
s	complex frequency [rad/sec]
F	force transmitted for force transmissibility elements [N]
V_o	voltage output [V]
V_i	voltage input [V]
η	hysteretic damping ratio
ω_n	natural frequency [rad/sec]
R	resistance [ohms]
t	time [s]
ζ	viscous damping ratio
E	elastic modulus [Pa]
A	rubber cross sectional area [$m^{2]}$
L_r	length of rubber piece [m]
F_{theo}	theoretical pole frequency [Hz]
F_{exp}	experimental pole frequency [Hz]
$\Delta\omega$	frequency range of resonance at $\frac{\max amplitude}{\sqrt{2}}$ [rad/sec]
K'	storage component of dynamic stiffness [N/mm]

K'' dissipative component of dynamic stiffness [N/mm]

K_d dynamic stiffness [N/mm]

Φ phase angle [degrees]

$f(t)$ input excitation force as a function of time [N]

$x(t)$ output displacement as a function of time [m]

$\dot{x}(t)$ output velocity as a function of time [m/s]

$\ddot{x}(t)$ output acceleration as a function of time [m/s^2]

j $\sqrt{-1}$

X amplitude of output displacement [m]

F_i amplitude of input excitation force [N]

$Y(s)$ input displacement for tuned mass damper as a function of complex frequency [m]

$F(s)$ output force for tuned mass damper as a function of complex frequency [N]